

7-8-2008

Enhancement of External Forced Convection by Ionic Wind

David Go

Raul A. Maturana

Timothy Fisher
tsfisher@purdue.edu

S V. Garimella
Purdue University, sureshg@purdue.edu

Follow this and additional works at: <http://docs.lib.purdue.edu/coolingpubs>

Go, David; Maturana, Raul A.; Fisher, Timothy; and Garimella, S V., "Enhancement of External Forced Convection by Ionic Wind" (2008). *CTRC Research Publications*. Paper 106.

<http://dx.doi.org/10.1016/j.ijheatmasstransfer.2008.05.012>

This document has been made available through Purdue e-Pubs, a service of the Purdue University Libraries. Please contact epubs@purdue.edu for additional information.

Enhancement of External Forced Convection by Ionic Wind

David B. Go, Raul A. Maturana, Timothy S. Fisher and Suresh V. Garimella

School of Mechanical Engineering and Birck Nanotechnology Center

Purdue University, West Lafayette, Indiana 47907 USA

Abstract

An ionic wind is formed when air ions are accelerated by an electric field and exchange momentum with neutral air molecules, causing air flow. Because ionic winds can generate flow with no moving parts and have low power consumption, they offer an attractive method for enhancing convection heat transfer from a surface. In the present work, corona discharges are generated between a steel wire and copper-tape electrode pair on a flat plate, perpendicular to the bulk flow direction such that the ensuing ionic wind is in the direction of the bulk flow. The corona discharge current is characterized, and experimental measurements of heat transfer from a flat plate are reported. Infrared images demonstrate that the cooling occurs along the entire length of the wire, and local heat transfer coefficients are shown to increase by more than 200% above those obtained from bulk flow alone. The magnitude of the corona current and the heat flux on the flat plate are varied. The heat transfer coefficient is shown to be related to the fourth root of the corona current both analytically and experimentally, and heat transfer enhancement is seen to be a solely hydrodynamic effect. Variation of the spacing between electrodes demonstrates that while the local peak enhancement is largely unaffected, the area of heat transfer enhancement is dependent on this spacing.

Nomenclature

$A_{current}$	cross-sectional area of ion current flow (m^2)
b	ion mobility in air ($m^2/V\cdot s$)
C_p	specific heat ($J/kg\cdot K$)
D_{IA}	mass diffusion coefficient of ions in air (m^2/s)
E	electric field (V/m)
f	body force (N/m^3)
G	electrode gap (mm)
H	electrode height (mm)
h	heat transfer coefficient ($W/m^2\cdot K$)
i	corona current (μA)
k	thermal conductivity ($W/m\cdot K$)
KE	kinetic energy (J)
L	plate length (mm)
Nu	Nusselt number

q''	heat flux (W/m ²)
p	pressure (N/m ²)
P	heater power (W)
Ra^*	Rayleigh number based on heat flux
Re	Reynolds number
T	temperature (K)
u	velocity (m/s)
x	distance along the plate (mm)

Greek symbols

ε	permittivity of air (F/m)
ν	kinematic viscosity (m ² /s)
ρ	mass density (kg/m ³)
ρ_e	air ion density (C/m ³)
σ	electrical conductivity of air ($\Omega^{-1}\text{m}^{-1}$)
Φ	applied corona potential (kV)

Subscripts

avg	average
bulk	due to bulk flow only
forced	forced convection
free	free (natural) convection
ionic	due to ionic wind only
∞	ambient air value

Superscript

*	based on heat flux
---	--------------------

Key Words: ionic wind, corona wind, corona discharge, electrohydrodynamics, forced convection, heat transfer enhancement

1. Introduction

Flow can be generated when air ions are accelerated through an interstitial atmosphere between two electrodes held at a potential difference. As the ions are acted upon by the electric field, they collide and exchange momentum with the neutral air molecules. At the millimeter scale, air ions can be generated by a dc corona discharge when a large voltage is applied between two electrodes, one sharp and the other blunt (collector electrode), in air. The electric field is geometrically enhanced very near the sharp electrode and

accelerates naturally occurring free electrons toward the electrode. These electrons collide with neutral molecules and, if the collision occurs at sufficiently high kinetic energy, strip electrons from the neutral molecule to form air ions. The air ions are then pulled by the field toward the blunt electrode, colliding with other neutral air molecules and forming what is typically called an ionic or corona wind. If the ionic wind is generated in the presence of a bulk flow, the ionic wind acts as a Coulombic body force on the bulk flow, adding momentum and disrupting the boundary layer (see Figure 1). In this work, we investigate the use of an ionic wind to distort the boundary layer of an external bulk flow. The modulated boundary layer increases heat transfer at the wall in a manner similar to a passive turbulator or blowing/suction at the wall.

The phenomenon of ionic wind was first studied by Chattock [1] in 1899, and in the mid-twentieth century, Stuetzer [2] and Robinson [3] extensively investigated the subject and developed the basic theory underlying electrohydrodynamic pumps. As a method for heat transfer enhancement, ionic winds can either provide forced convection in environments that would otherwise be cooled only by natural convection and/or radiation, or enhance forced convection as discussed above. Marco and Velkoff [4] pioneered this research by examining enhanced natural convection using an ionic wind generated by a wire (sharp) electrode impinging on a plate (blunt) electrode. Similar point-to-plane configurations have been studied by Kibler and Carter [5] as well as Owsenek and Seyed-Yagoobi [6] and Owsenek et al.[7] The use of a corona discharge as a blower for duct flow between two plates (or fins) has also been suggested by Kalman and Sher [8] and Jewell-Larsen et al. [9]. Forced convection enhancement has been studied extensively for both laminar and turbulent internal flows [10][11][12]. Additionally, ionic-wind-enhanced heat transfer has been investigated by Ohadi et al. [13] for a shell-and-tube heat exchanger and by Wangnipparnto et al. [14] in a thermosyphon heat exchanger.

The use of ionic winds in the presence of a bulk flow to modulate an external boundary layer has been an area of growing interest in the aerospace community, but has received little attention for heat transfer enhancement. Soetomo [15], and more recently, Léger et al. [16] and Artana et al. [17], demonstrated the ability of corona discharges to reduce drag by modulating the boundary layer on a flat plate. Using electrodes perpendicular to the flow and either flush or in contact with a flat plate, they demonstrated a near-wall ionic wind that accelerates the local boundary layer, promoting drag reduction. The only experiments reported in the literature on heat transfer enhancement by ionic winds in the presence of external flows were by Velkoff and Godfrey [18], who used an array of corona wires aligned with the flow and extended above a flat plate. With the flat plate acting as the collecting electrode, they demonstrated that heat transfer is enhanced in the low-velocity regime but that the ionic wind is swamped by the bulk flow, and thus ineffective, as the bulk velocity increases.

Recently, ionic wind devices reduced to microscale dimensions have been proposed for on-chip thermal management of electronic devices [19][20]. As the electrode gap is decreased to 10-20 μm , the ionization

phenomenon is no longer due to the acceleration of free electrons (*i.e.*, corona discharge) but rather the injection of electrons into air from the cathode by field emission. Our group has previously modeled and studied the ionization process [21][22] and demonstrated that, by using nanostructured carbon for geometric field enhancement, emission turn-on voltages can be reduced to approximately 20 V [23]. Whereas these studies explored microscale ionic winds to generate air under otherwise quiescent conditions, the focus of more recent work has been on the efficacy of using ionic winds for local heat transfer enhancement in existing bulk flows [24]. Recent experiments have revealed that ionic winds can increase the local heat transfer coefficient in an externally generated, low-velocity bulk flow over a flat plate by more than a factor of 2 for applied voltages of 2 to 4 kV [25]. The present work focuses on the correlation between ion current and heat transfer enhancement under different geometric arrangements.

2. Theory of Electrohydrodynamics

The interaction between ions and neutral molecules is typically called ion drag and is defined using the following body force equation consisting of the Coulombic force, the force due to the permittivity gradient and the electrostriction force:

$$\vec{f} = \rho_e \vec{E} - \frac{1}{2} |E|^2 \vec{\nabla} \varepsilon + \frac{1}{2} \vec{\nabla} \left[|E|^2 \rho \frac{\partial \varepsilon}{\partial \rho} \right] \quad (1)$$

Electrostriction is only significant in cases in which a two-phase interface exists [6]. Also, the permittivity gradient is negligible in air. Therefore, ion drag in air is due only to the Coulombic force ($\rho_e \vec{E}$) and is included in the standard momentum equation as a body force term:

$$\vec{\nabla} \cdot (\rho \vec{u} \vec{u}) = -\vec{\nabla} p + \nu \nabla^2 \vec{u} + \rho_e \vec{E} \quad (2)$$

In addition to the exchange of kinetic energy, the ion current imparts thermal energy to the air, and this phenomenon is included in the energy equation as a Joule heating term:

$$\vec{u} \cdot \vec{\nabla} (\rho C_p T) = k \nabla^2 T + b \rho_e E^2 - \vec{u} \cdot (\rho_e \vec{E}) \quad (3)$$

The second term on the right side of Eq. (3) is the Joule heating term [6], and the last term subtracts the kinetic work that the ions impart to the flow because not all ion energy is converted to heat. In previous work, modeling of the ion current and electrohydrodynamic interactions suggested that Joule heating can result in upstream heating of the flow at low ion currents [25].

Once the ions are generated by electron impact in the corona discharge, they can be transported through the interstitial medium by four mechanisms (charge diffusion, drift, convection and mass diffusion) as described by the following equation.

$$\vec{\nabla} \cdot (\sigma \vec{E} + b \vec{E} \rho_e + \vec{u} \rho_e) = D_{IA} \nabla^2 \rho_e \quad (4)$$

The charge diffusion and drift of ions through the air are driven by the applied electric field, though the electrical conductivity of air is small ($\sigma \approx 1.61 \times 10^{-23} \Omega^{-1} \text{m}^{-1}$ [26]) and electrical charge diffusion is

negligible. The convection of ions is due to the velocity of the bulk flow but it is often small when compared to the ion drift velocity induced by the electric field [6]. The term on the right side of the equation is the mass diffusion of the ions, though it is typically negligible when compared to drift. The electric field is described classically by Poisson's equation

$$\bar{\nabla} \cdot \bar{E} = -\nabla^2 \Phi = \frac{\rho_e}{\epsilon} \quad (5)$$

The term on the right side is a charge-screening term that can distort the electric field when the ion current is very large and the ion density is significant. The above equations describe the continuum-scale interactions between the fluid and the ions in the flow region between the sharp and collecting electrodes. It should be noted that the corona discharge and ion generation very near the sharp electrode is a microscale phenomena and, generally, the physics in this localized region are not accurately described by the continuum-scale equations.

3. Experimental Setup

The experimental setup used in the current work is shown in Figure 2, and consists of a flat plate exposed to a bulk flow with the corona electrodes oriented perpendicular to the flow such that the discharge current and ensuing ionic wind are aligned with the flow. The flat plate is made of 0.7 mm thick glass with a thin layer of indium tin oxide (ITO) present on its underside. Electrodes were attached to the ITO layer using silver epoxy, and a potential was applied to heat the flat plate. In order to isolate the two electrodes that form the corona electrode pair, the top of the flat plate was coated with 0.127 mm-thick teflon. The ITO heater was insulated on the back side with Styrofoam. The bulk flow was generated with an axial fan, and 50.8 mm-thick honeycomb with 3.175 mm cells was placed upstream of the flat plate to condition the flow. Two parallel polycarbonate plates were used to prevent the flow from spreading laterally. The bulk velocities investigated were less than 1 m/s, and by defining the Reynolds number as

$$\text{Re} = \frac{uL}{\nu} \quad (6)$$

it follows that the experimental flow regime was entirely laminar ($\text{Re} < 10^4$ based on a plate length of $L = 125$ mm) for the conditions of these tests.

A corona discharge was generated between a 50 μm -diameter stainless steel wire anode (corona wire) and a 6.35 mm-wide copper tape cathode (collecting electrode) attached to the flat plate. The corona wire was strung across the flow upstream of the collecting electrode and elevated above the flat plate by two ceramic blocks. The collecting electrode was placed 55.25 mm downstream of the leading edge of the flat plate, and this position was held constant. The height (H) of the elevated corona wire was held constant at 3.15 mm and the gap (G) between the two electrodes was varied in the experiments.

Thermal measurements were obtained with a FLIR ThermoCAM SC300 infrared (IR) camera located above the flat plate. The accuracy of the camera was assessed to be ± 1 °C over the range of 30-70 °C using a blackbody calibrator. The flat plate was painted with Krylon Ultra Flat Black Spray 1602, which has a known emissivity of 0.96 [27], to ensure accurate IR readings. The bulk flow velocity was measured at the collecting electrode with a hand-held velocimeter with an estimated accuracy of ± 0.05 m/s. The corona discharge was generated by applying a voltage to the corona wire while the collecting electrode was grounded. The corona current was measured at the collecting electrode using a picoammeter.

4. Results and Discussion

4.1 Corona Discharge Characterization

Stuetzer [2] analytically predicted that for plane, cylindrical, or spherical electrodes, the relationship between the applied potential (Φ) and the resulting corona current (i) should follow

$$i^{1/2} \propto \Phi \quad (7)$$

This relationship was previously demonstrated experimentally for point-to-plane geometries by both Kibler and Carter [5] as well as Owsenek et al. [7]. Figure 3 contains a plot of the square root of the corona current as a function of the applied potential for electrode spacings of $G = 0, 2, 4,$ and 6 mm at a constant corona wire height of $H = 3.15$ mm. The plot confirms the linear relationship between the square root of current and the voltage in this geometric configuration. Additionally, for a given applied voltage, the magnitude of the corona current increases as the gap between electrodes decreases. Ions are formed by sufficiently energetic electrons colliding with neutral molecules and stripping electrons. The Coulombic force accelerating the electrons is due to the electric field, which is related to the gradient of the applied potential as shown in Eq. (5). Therefore, as the gap decreases at a given applied potential, the electric field increases as does the kinetic energy imparted to the electrons. With a greater number of highly energetic electrons, the ionization is enhanced; therefore the ensuing ion current is greater.

4.2 Heat Transfer Characterization

Figure 4 shows a series of infrared thermal contour images for a flat plate heater power of $P = 4$ W. The image at the top shows the heated plate prior to any forced convection cooling. The second image corresponds to the heated plate exposed to a $u = 0.28$ m/s bulk flow. The final image is of the heated plate with a corona discharge-generated ionic wind in the presence of the bulk flow, where the ion current is aligned with the flow. The electrode geometry was $H = 3.15$ mm and $G = 2.0$ mm, and the corona discharge occurred under an applied potential of 4.51 kV, producing a current of 15 μ A. Under these corona conditions, significant cooling enhancement occurs in the vicinity of the corona wire as well as downstream of the collecting electrode. To a lesser extent, convection enhancement also exists upstream of the electrode pair.

Because the corona discharge and cooling occur relatively uniformly along the spanwise length of the wire, the heat transfer effect is largely two-dimensional (x-y) along the direction of flow. Therefore, the temperatures from a single streamwise line along the plate were analyzed to determine heat transfer coefficients. The local heat transfer coefficient was calculated based on the known heater input power and the estimated radiative heat loss from the surface as

$$h_x = \frac{q''_{\text{heater}} - q''_{\text{plate, radiation}}}{T_{\text{plate, x}} - T_{\infty}} \quad (8)$$

In order to separate the local heat transfer enhancement produced by the ionic wind in the presence of the bulk flow from that due to the bulk flow itself, a local percentage improvement in the local heat transfer coefficient is defined as

$$\Gamma_x = \frac{(h_{x, \text{bulk+ionic}} - h_{x, \text{bulk}})}{h_{x, \text{bulk}}} \times 100 \quad (9)$$

Average upstream and downstream heat transfer coefficients were determined from the local data as

$$h_{\text{avg}} = \frac{1}{\Delta x} \int_{x_1}^{x_2} h_x dx \quad (10)$$

The upstream value was based on a 5 mm-long region upstream of the collecting electrode ($x = 50\text{-}55$ mm), and the downstream value was based on a 5 mm-long region downstream of the collecting electrode ($x = 62\text{-}67$ mm); the collecting electrode stretches from $x = 55.25\text{-}61.60$ mm. The uncertainty in the calculated average heat transfer coefficients was observed to vary between 4% at smaller values of h_{avg} to approximately 8% at larger h_{avg} values based on the $\pm 1^\circ\text{C}$ accuracy of the camera and standard error-propagation analysis [28]. The uncertainty is presented as error bars in the figures.

While a simple expression for local natural convection on heated horizontal plates is not available, natural convection can be accounted for when calculating average heat transfer coefficients. The measured average heat transfer coefficient as defined in Eq. (10) can be written as a summation of the free convection and forced convection components using the following relationship for transverse flows [29]

$$h_{\text{avg}}^{7/2} = h_{\text{forced}}^{7/2} + h_{\text{free}}^{7/2} \quad (11)$$

The forced convection component here includes both the bulk flow and ionic wind components, while the free convection value was estimated using the correlation [30]

$$\overline{Nu} = 0.61 (Ra^*)^{1/5} \quad (12)$$

where the Rayleigh number, Ra^* , is based on the known heat flux at the flat plate.

With bulk flow only, the forced convection coefficient in Eq. (11) is simply

$$h_{\text{forced}} = h_{\text{bulk}} \quad (13)$$

However, when the ionic wind is activated, the forced convection coefficient consists of both the underlying bulk flow component and the ionic wind component, and their relative contributions can be estimated using the following relationship for assisting flows [29] (where h_{bulk} is considered constant with and without the ionic wind active).

$$h_{forced}^3 = h_{bulk}^3 + h_{ionic}^3 \quad (14)$$

Equations (10)-(14) were used to determine the contribution due to ionic wind in the measured heat transfer enhancement in the results presented below.

4.3 Heat Transfer Enhancement

Experiments were conducted with varying magnitudes of the corona current and the heat flux on the flat plate in order to understand the nature of the interaction of the ionic wind with the bulk flow and its effects on heat transfer. Additional experiments were conducted to explore the impact on heat transfer of the geometric spacing between the corona wire and the collecting electrode.

Figure 5 shows the percentage increase in the local heat transfer coefficient as defined by Eq. (9) for bulk flow in the presence of an active ionic wind. The peak value is greater than 200% for a corona current of 15 μA (or 67.6 mW of electrical input power), and the local enhancement decreases to 50% for a current of 3 μA (10.6 mW). Heat transfer enhancement occurs both upstream and downstream of the electrode pair and peaks at the location of the corona wire. The upstream enhancement is not as large as the downstream enhancement, and for low currents, modest upstream heating is observed when localized Joule heating can become significant [25]. The enhancement decreases steadily with increased downstream distance from the collecting electrode as the ionic wind is dissipated. The two shaded regions represent the upstream and downstream areas over which h_{avg} values were calculated as defined in Eq. (10).

Previous work by the authors [24] suggested that the heat transfer coefficient is proportional to the fourth root of the Coulombic body force. Because the main transport mechanism of ions in air is drift, as opposed to conduction or convection by the bulk flow, the ion current is defined as

$$i = (b\rho_e \vec{E}) A_{current} \quad (15)$$

where $A_{current}$ is the cross-sectional area of the ion flow. Equation (1) shows that the body force is proportional to the ion density and the electric field. Assuming that the ion mobility and cross-sectional area are constant, the current is proportional to the body force and thus proportional to the kinetic energy imparted to the flow

$$i \propto \vec{f} \propto KE \quad (16)$$

In turn, kinetic energy is proportional to the square of velocity, and it follows that the velocity is proportional to the square-root of current

$$v \propto i^{1/2} \quad (17)$$

The relationship between heat transfer coefficient and free-stream velocity in external, laminar flows is known analytically [29]

$$h \propto v^{1/2} \quad (18)$$

It follows from these relationships that the heat transfer coefficient due to the ionic wind should be proportional to the fourth-root of the corona current, $h_{ionic} \propto i^{1/4}$. This relationship especially holds true if the current is reasonably large and the primary effect of the ionic wind is to add momentum to the bulk flow, in which case the enhancement is hydrodynamic rather than an electrically induced thermal effect (*i.e.*, the impact of Joule heating on pressure and air properties is small and negligible).

Figure 6 shows the average heat transfer coefficient due to the ionic wind, h_{ionic} from Eq. (14), as a function of the fourth root of corona current. The relationship is predominantly linear across the various corona conditions for both upstream and downstream heat transfer coefficients, and therefore confirms the relationship suggested above. This observation further indicates that, in the region over which h_{ionic} was calculated, the kinetic energy imparted to the flow by the ionic wind is more significant than Joule heating. However, if the region over which h_{ionic} was calculated were expanded upstream, this relationship may not hold as Joule heating is significant in the $i = 3 \mu\text{A}$ case. Figure 6 also reveals a cross-over between the upstream and downstream curves at low currents, where the downstream enhancement exceeds that upstream. This trend is also apparent in Figure 5. The peak enhancement location for curves (a)-(d) in this figure is in the vicinity of the corona wire and decreases downstream of the collecting electrode. However, the peak in curve (e) is not at the corona wire location. While further study is required to understand the precise physical mechanisms that govern this observation, this characteristic may be exploited in practical designs.

Because the primary mechanism for heat transfer enhancement is assumed to be momentum addition, as shown above, the measured heat transfer coefficients should be independent of the magnitude of the heat flux imposed on the flat plate. Figure 7 shows the upstream and downstream measurements of h_{bulk} and h_{ionic} for varying power inputs to the heated plate, but at a fixed ion current of $15 \mu\text{A}$. The average heat transfer coefficients are largely constant to within experimental uncertainty across the range of power inputs, again confirming this assumption. The slight increasing trend with heater power might be attributable to inaccuracies in the natural convection correlation. Additionally, the ionic wind heat transfer coefficients are approximately three times those of the bulk flow alone at these conditions.

A parametric study was also conducted in which the gap (G) between the corona wire and collecting electrode were varied. The corona wire was maintained at a constant elevation, $H = 3.15 \text{ mm}$, and each geometric configuration was operated at the same corona current of $15 \mu\text{A}$, although the applied voltage increased with the gap spacing from to 4.39 kV at $G = 1 \text{ mm}$ to 6.15 kV at $G = 5 \text{ mm}$. Figure 8 shows the relative increase in

the local heat transfer coefficient, as defined by Eq. (9), for three different electrode gaps. It is noted that the peak magnitude of heat transfer enhancement does not vary appreciably for the electrode gaps considered and still occurs in the vicinity of the corona wire. While the general trend of upstream and downstream enhancement is consistent across the range of electrode gaps, the magnitude of enhancement increases as the electrode gap increases. This effect is particularly apparent upstream of the corona wire where the local enhancement is more pronounced at $G = 5$ mm than at $G = 1$ mm. From a design perspective, the peak heat transfer enhancement is nearly the same at $G = 1$ mm as that at $G = 5$ mm but requires approximately 2 kV less of applied potential, or nearly 30% less electrical power; however, the total area of heat transfer enhancement is greater at larger gaps.

5. Conclusions

Enhancement of forced convection heat transfer using an ionic wind has been demonstrated. The corona discharge current was shown to be quadratically related to the applied voltage, confirming theory and observations by earlier investigators. An increase of more than 200% was observed in the local heat transfer coefficient due to the ionic wind for a power input of 67.6 mW, and the heat transfer coefficient was shown to vary linearly with the fourth root of the corona current, confirming the expected relationship based on analysis. Little variation of the ionic wind heat transfer coefficient with the heat flux imposed on the plate was observed, which suggests that the electrohydrodynamic interaction is due to largely hydrodynamic effects rather than electrically induced thermal effects. Experiments with different electrode gaps reveal slight changes in both upstream and downstream enhancement but consistency in terms of the location of maximum enhancement near the corona wire.

Acknowledgement

The authors would like to acknowledge technical discussions and financial support from Intel Corporation.

References

- [1] A. Chattock, On the velocity and mass of ions in the electric wind in air, *Philos. Mag.*, **48** (1899), pp. 401-420.
- [2] O. Stuetzer, Ion drag pressure generation, *J. Applied Physics* **30** (1959), pp. 984-994.
- [3] M. Robinson, Movement of air in the electric wind of the corona discharge, *Trans. of the Am. Inst. Elec. Eng. Comm. Elec. (AIEE J.)* (1961), pp. 143-150.
- [4] S. M. Marco, H. R. Velkoff, Effect of electrostatic fields on free convection heat transfer, *ASME Paper No. 63-HT-9* (1963).
- [5] K. G. Kibler, H. G. Carter Jr., Electrocooling in gases, *J. Appl. Physics* **45** (1974), pp. 4436-4440.
- [6] B. L. Owsenek, J. Seyed-Yagoobi, Theoretical and experimental study of electrohydrodynamic heat transfer enhancement through wire-plate corona discharge, *J. Heat Transfer* **119** (1997), pp. 604-610.
- [7] B. L. Owsenek, J. Seyed-Yagoobi, R. H. Page Experimental investigation of corona wind heat transfer enhancement with a heated horizontal flat plate, *J. Heat Transfer* **117** (1995), pp. 309-315.
- [8] H. Kalman, E. Sher, Enhancement of heat transfer by means of a corona wind created by a wire electrode and confined wings assembly, *Appl. Thermal Eng.* **21** (2001), pp. 265-282.
- [9] N. E. Jewell-Larsen, E. Tran, I. A. Krichtafovitch, A. V. Mamishev, Design and optimization of electrostatic fluid accelerators, *IEEE Trans. Dielectrics and Electrical Insulation* **13** (2006), pp. 191-203.
- [10] A. Takimoto, Y. Tada, Y. Hayashi, K. Yamada, Convective heat transfer enhancement by a corona discharge, *Heat Transfer: Japanese Research* **20** (1991), pp. 19-35.
- [11] D. A. Nelson, S. Zia, R. L. Whipple, M. M. Ohadi, Corona discharge effects on heat transfer and pressure drop in tube flows, *Enhanced Heat Transfer* **7** (1998), pp. 81-95.
- [12] M. Molki, K. L. Bhamidipati, Enhancement of convective heat transfer in the developing region of circular tubes using corona wind, *Int. J. Heat Mass Transfer* **47** (2004), pp. 4301-4314.
- [13] M. M. Ohadi, D. A. Nelson, S. Zia, Heat transfer enhancement of laminar and turbulent pipe flow via corona discharge, *Int. J. Heat Mass Transfer* **34** (1991), pp. 1175-1187.
- [14] S. Wangnipparnto, J. Tiansuwan, S. Jiracheewanun, T. Kiatsiriroat, C. C. Wang, Air side performance of thermosyphon heat exchanger in low Reynolds number region: with and without electric field, *Energy Conversion Management* **43** (2002), pp. 1791-1800.
- [15] F. Soetomo, The influence of high voltage discharge on flat plate drag at low Reynolds number air flow, M.S. Thesis, Iowa State University, Ames, IA, 1992.
- [16] L. Léger, E. Moreau, G. Touchard, Control of low velocity airflow along a flat plate with a dc electrical discharge, *IEEE Trans. Industrial Appl.* **38** (2002), pp. 1478-1485.
- [17] G. Artana, J. D'Adamo, L. Léger, E. Moreau, G. Touchard, Flow control with electrohydrodynamic actuators, *AIAA J.* **40** (2002), pp. 1773-1779.
- [18] H. R. Velkoff, R. Godfrey, Low-velocity heat transfer to a flat plate in the presence of a corona discharge in air, *J. Heat Transfer* **101** (1979), pp. 157-163.

- [19] D. J. Schlitz, S. V. Garimella, T. S. Fisher, Microscale ion-driven air flow over a flat plate, HT-FED04-56470, Proceedings of ASME Heat Transfer/Fluids Engineering Summer Conference, Charlotte, NC, July 2004.
- [20] C. P. Hsu, N. E. Jewell-Larsen, I. A. Krichtafovitch, S. W. Montgomery, J. T. Dibene II, A. V. Mamishev, Miniaturization of electrostatic fluid accelerators, *J. Microelectromech. Sys.* **16** (2007), pp. 809-815.
- [21] W. Zhang, T. S. Fisher, S. V. Garimella, Simulation of ion generation and breakdown in atmospheric air, *J. Appl. Physics* **96** (2004), pp. 6066-6072.
- [22] D. B. Go, T. S. Fisher, S. V. Garimella, Direct simulation Monte Carlo analysis of microscale field emission and ionization of atmospheric air, IMECE 2006-14476, Proceedings of ASME International Mechanical Engineering Congress and Exposition, Chicago, IL, 2006.
- [23] M. S. Peterson, W. Zhang, T. S. Fisher, S. V. Garimella, Low-voltage ionization of air with carbon-based materials, *Plasma Sources Sci. Tech.* **14** (2005), pp. 654-660.
- [24] D. B. Go, S. V. Garimella, T. S. Fisher, Numerical simulation of microscale ionic wind for local cooling enhancement, Proceedings of Tenth Intersociety Conference on Thermal and Thermomechanical Phenomena in Electrical Systems, San Diego, CA, 2006.
- [25] D. B. Go, T. S. Fisher, and S. V. Garimella, Ionic winds for locally enhanced cooling, *Journal of Applied Physics* – accepted for publication
- [26] M. Boulos, P. Fauchais, and E. Pfender, *Thermal Plasmas: Fundamentals and Applications* (vol. 1), Plenum Press, New York, 1994.
- [27] NASA, Data on the emissivity of a variety of black paints, <http://masterweb.jpl.nasa.gov/reference/paints.htm>, 2003 (accessed August 22, 2006)
- [28] J. R. Taylor, *An Introduction to Error Analysis* (second ed.), University Science Books, California, 1997, ch. 2.
- [29] F. P. Incropera, D. P. Dewitt, *Fundamentals of Heat and Mass Transfer* (fifth ed.), John Wiley & Sons, New York, 2002, pp. 393,568.
- [30] A. Bejan, *Convection Heat Transfer* (third ed.), John Wiley & Sons, New York, 2004.

Figures

Figure 1 Schematic showing an ionic wind generator in the presence of a bulk flow.

Figure 2 Experimental configuration for a flat plate exposed to a bulk flow and corona electrodes perpendicular to the flow.

Figure 3 Square root of the measured corona current as a function of the applied voltage for electrode gaps of $G = 0, 2, 4,$ and 6 mm. The corona wire was elevated 3.15 mm above the surface.

Figure 4 Infrared temperature contours ($^{\circ}\text{C}$) for a heater power of $P = 4$ W and three cooling conditions for a geometry of $H = 3.15$ mm and $G = 2.0$ mm. The bold, dashed line in the third image indicates the streamwise line along which individual temperatures were extracted and calculations conducted.

Figure 5 Percentage increase in local heat transfer coefficient for five corona conditions as a function of distance along the plate for a geometry of $H = 3.15$ mm and $G = 2.0$ mm. The bulk velocity was $u = 0.28$ m/s, and the heater power was $P = 4$ W. The blue line and red dot represent the collecting electrode and corona wire positions. The two shaded regions represent the upstream and downstream area over which h_{avg} was calculated.

Figure 6 The average ionic wind heat transfer coefficient as a function of the fourth root of the corona current. The bulk velocity was $u = 0.28$ m/s, and the heater power was $P = 4$ W. Linear fits show the relationship between the heat transfer coefficient and current.

Figure 7 Average bulk and ionic wind heat transfer coefficients as a function of the input heater power to the flat plate. The bulk velocity was $u = 0.28$ m/s, and the current was $i = 15$ μA . Linear fits show the relationship between the heat transfer coefficient and heater power.

Figure 8 Percentage increase in local heat transfer coefficient for three electrode gaps at a constant electrode height of $H = 3.15$ mm. The bulk velocity was $u = 0.28$ m/s, and the heater power was $P = 4$ W. The blue

line represents the collecting electrode, and the three dots represent the different positions of the corona wire for different electrode gaps.

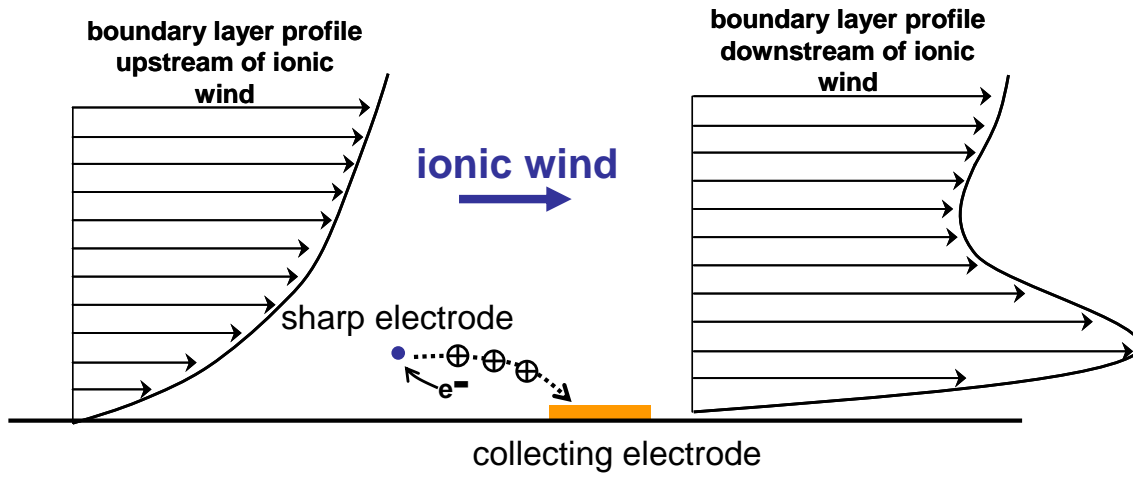


Figure 1 Schematic showing an ionic wind generator in the presence of a bulk flow.

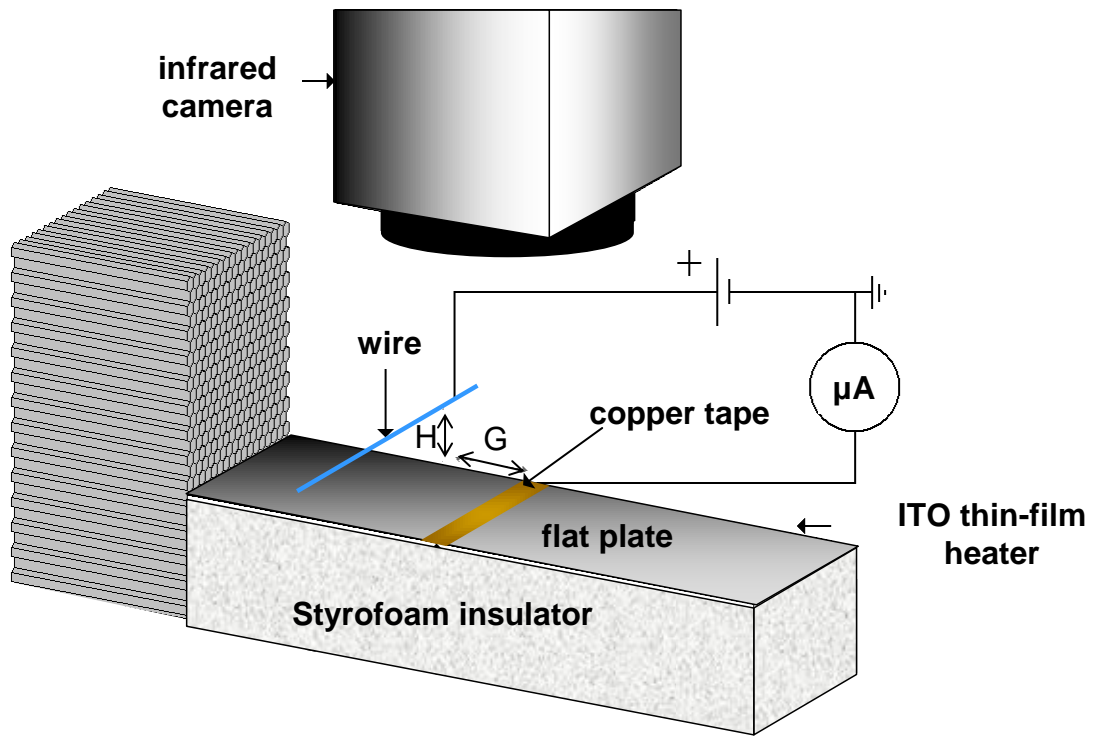


Figure 2 Experimental configuration for a flat plate exposed to a bulk flow and corona electrodes perpendicular to the flow.

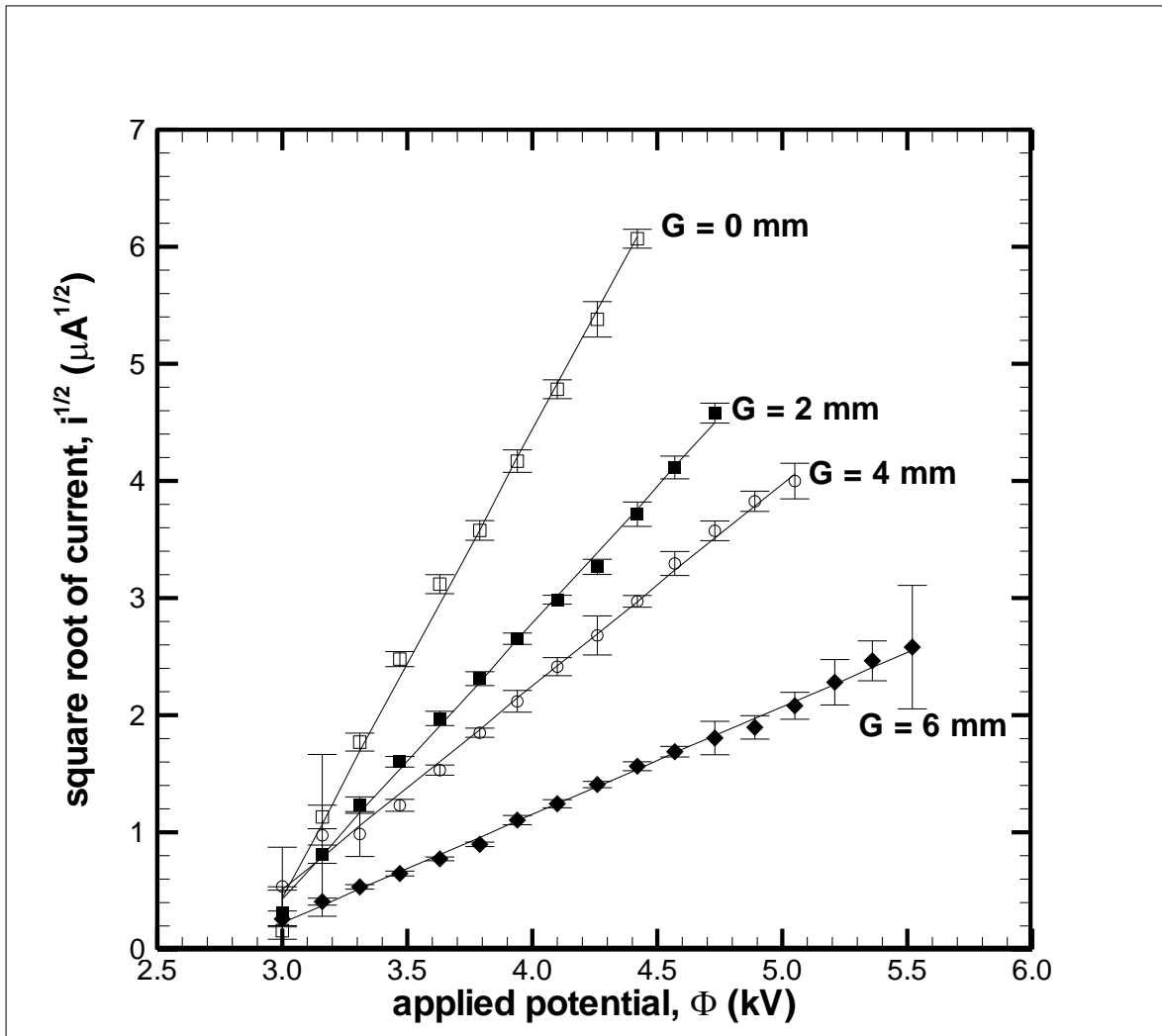


Figure 3 Square root of the measured corona current as a function of the applied voltage for electrode gaps of $G = 0, 2, 4,$ and 6 mm. The corona wire was elevated 3.15 mm above the surface.

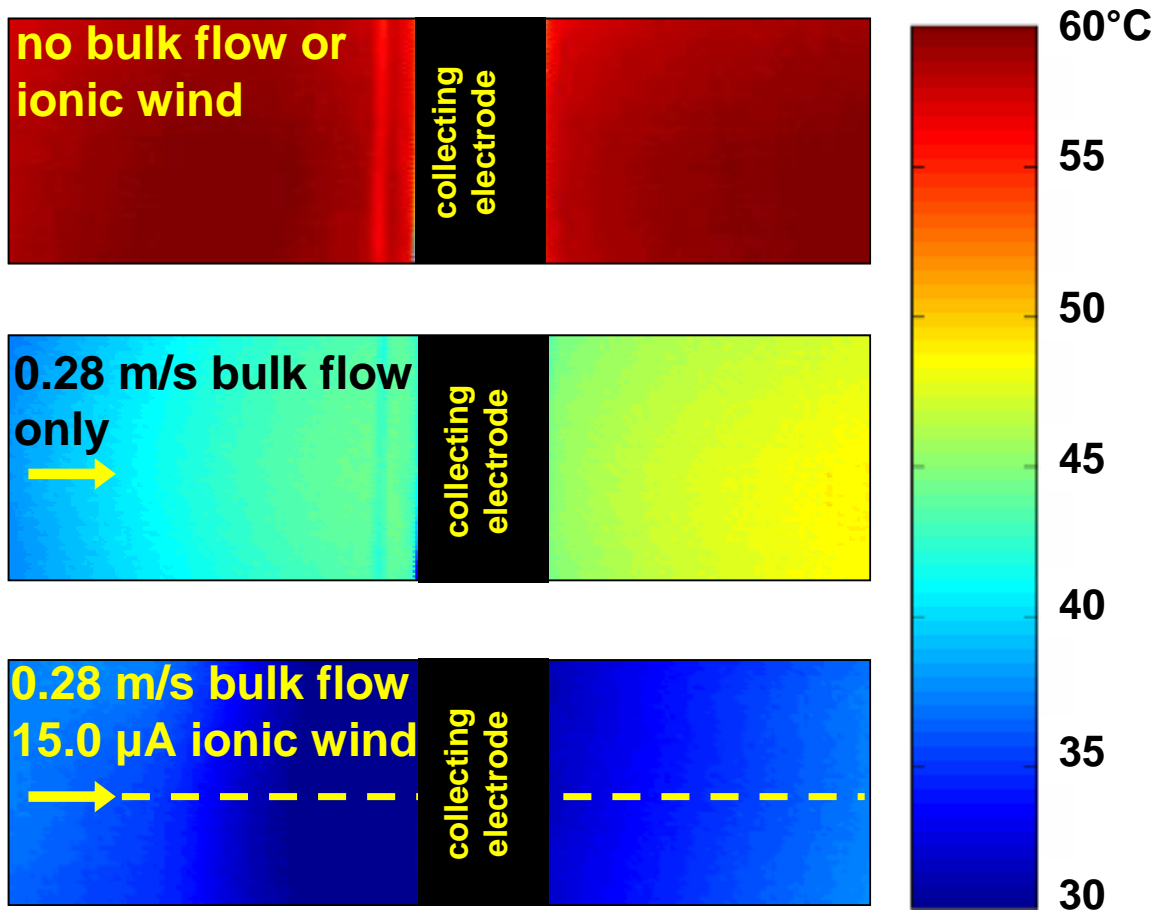


Figure 4 Infrared temperature contours ($^{\circ}\text{C}$) for a heater power of $P = 4$ W and three cooling conditions for a geometry of $H = 3.15$ mm and $G = 2.0$ mm. The bold, dashed line in the third image indicates the streamwise line along which individual temperatures were extracted and calculations conducted.

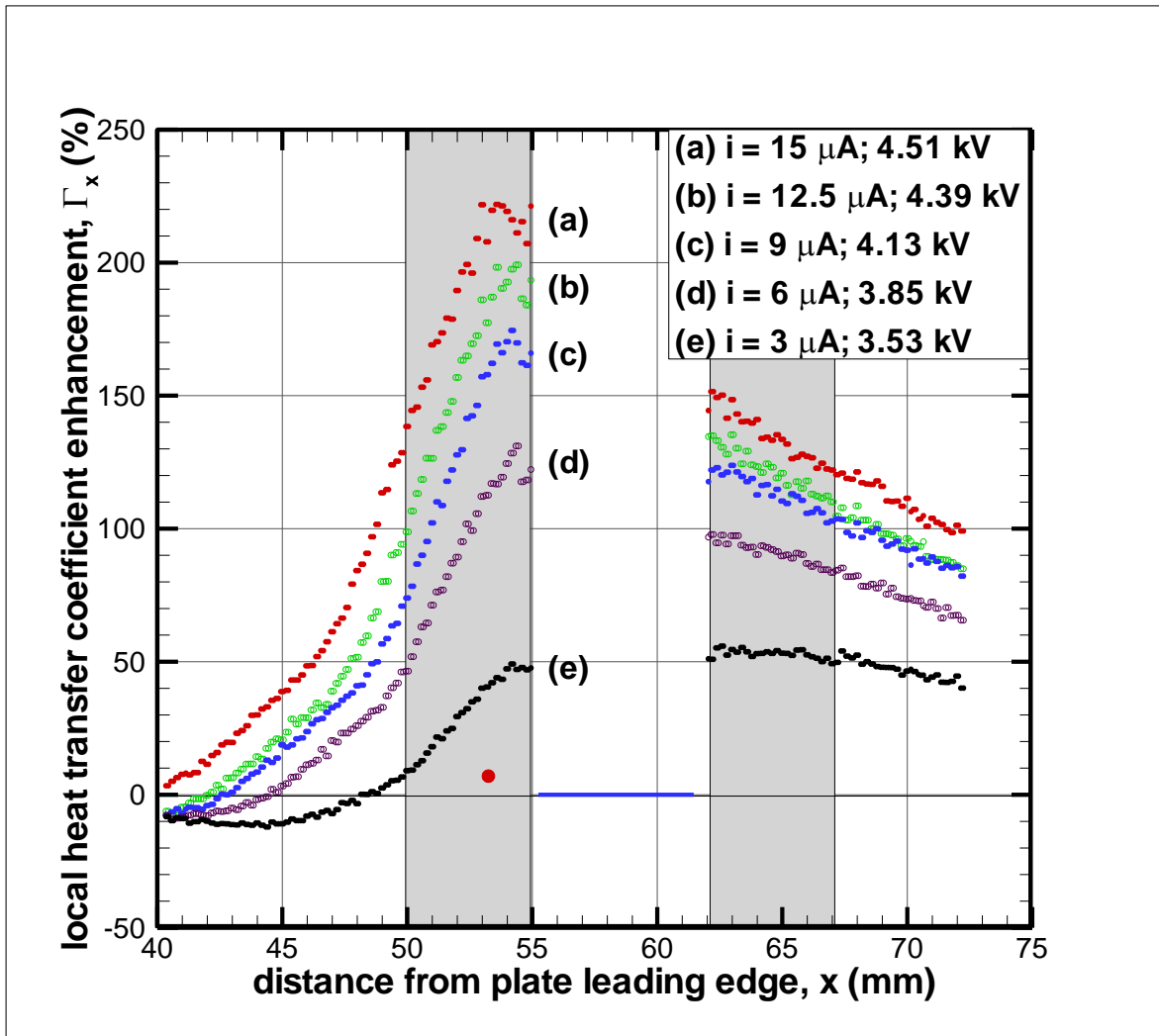


Figure 5 Percentage increase in local heat transfer coefficient for five corona conditions as a function of distance along the plate for a geometry of $H = 3.15$ mm and $G = 2.0$ mm. The bulk velocity was $u = 0.28$ m/s, and the heater power was $P = 4$ W. The blue line and red dot represent the collecting electrode and corona wire positions. The two shaded regions represent the upstream and downstream area over which h_{avg} was calculated.

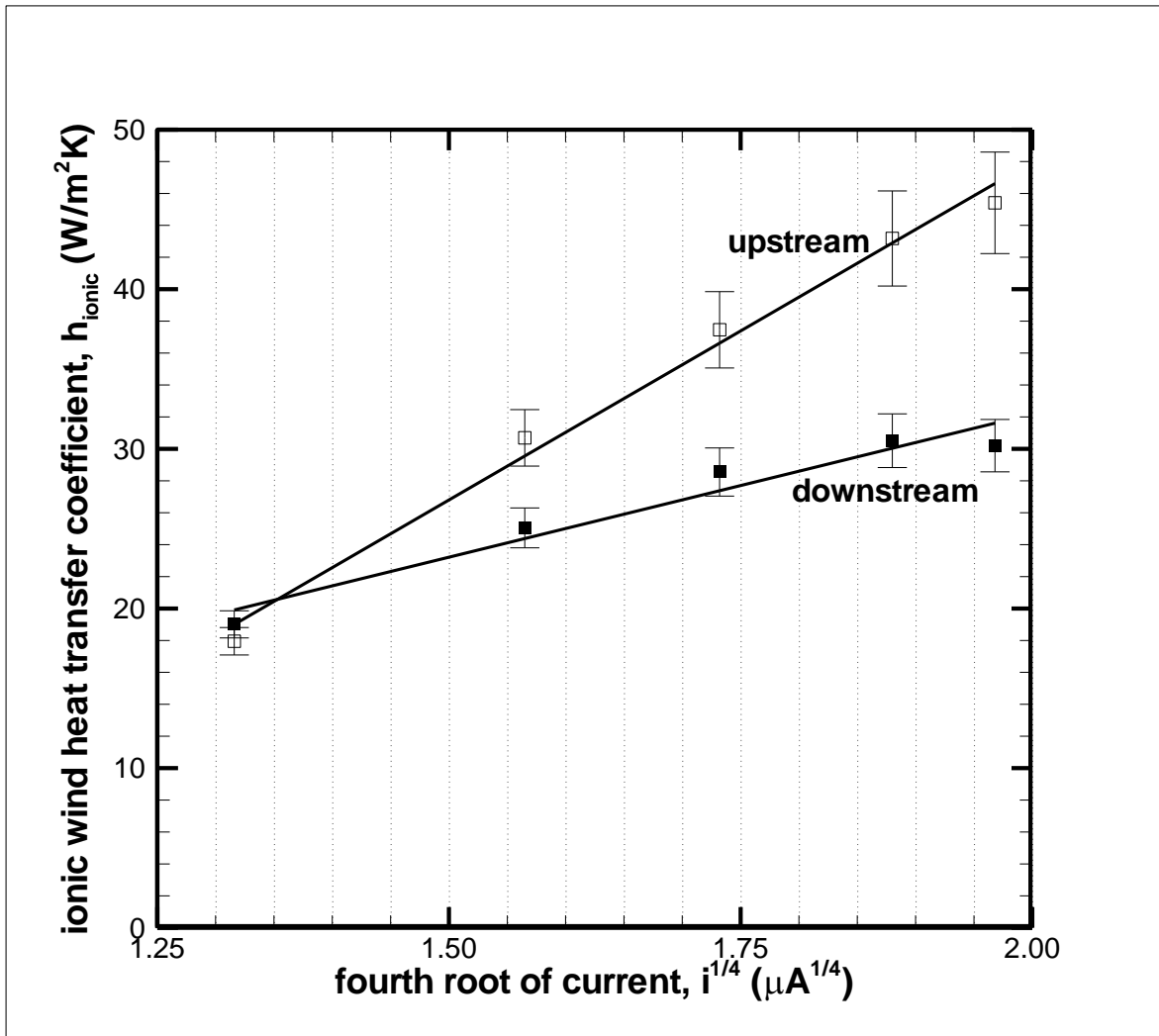


Figure 6 The average ionic wind heat transfer coefficient as a function of the fourth root of the corona current. The bulk velocity was $u = 0.28$ m/s, and the heater power was $P = 4$ W. Linear fits show the relationship between the heat transfer coefficient and current.

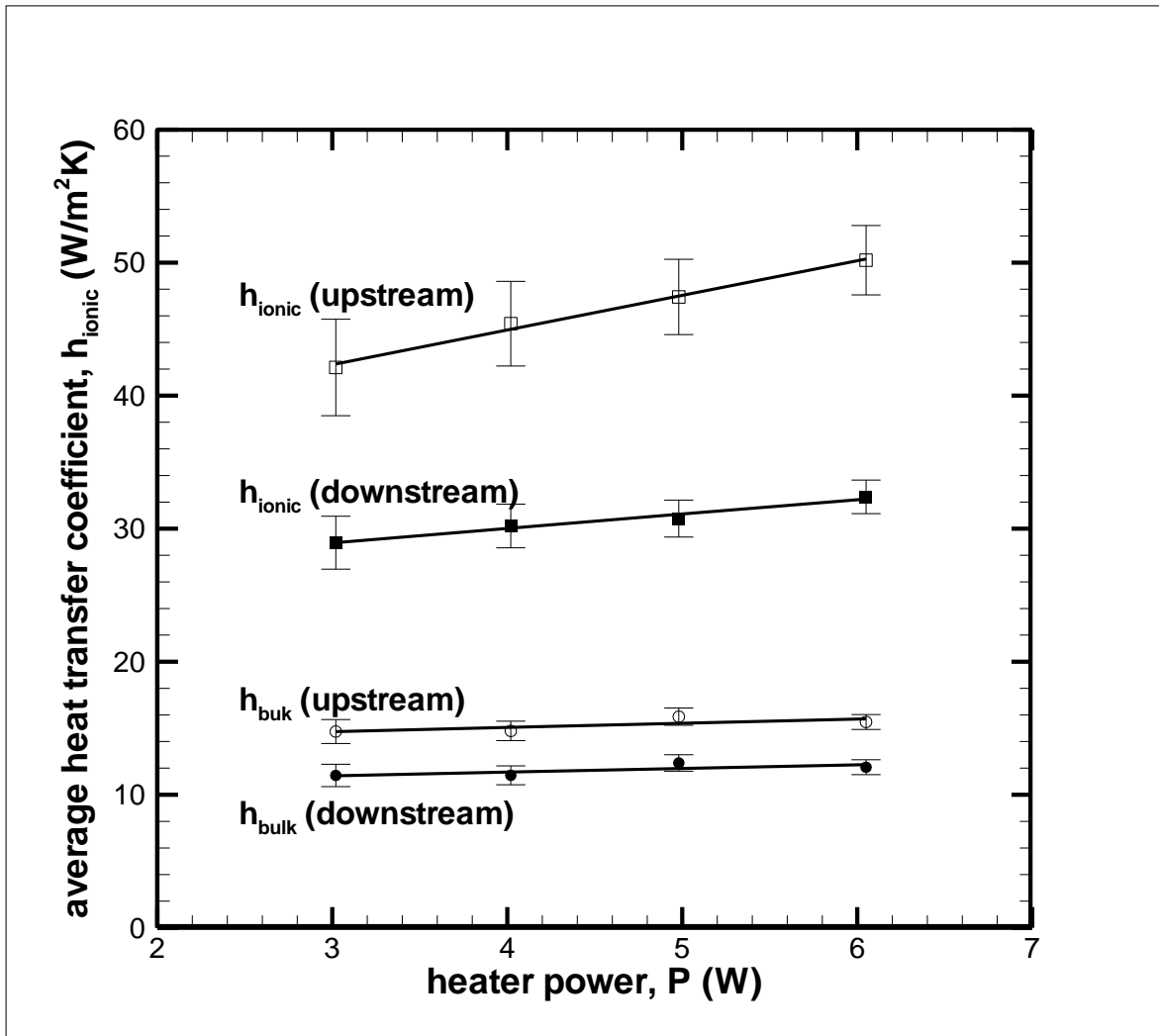


Figure 7 Average bulk and ionic wind heat transfer coefficients as a function of the input heater power to the flat plate. The bulk velocity was $u = 0.28$ m/s, and the current was $i = 15$ μ A. Linear fits show the relationship between the heat transfer coefficient and heater **power**.

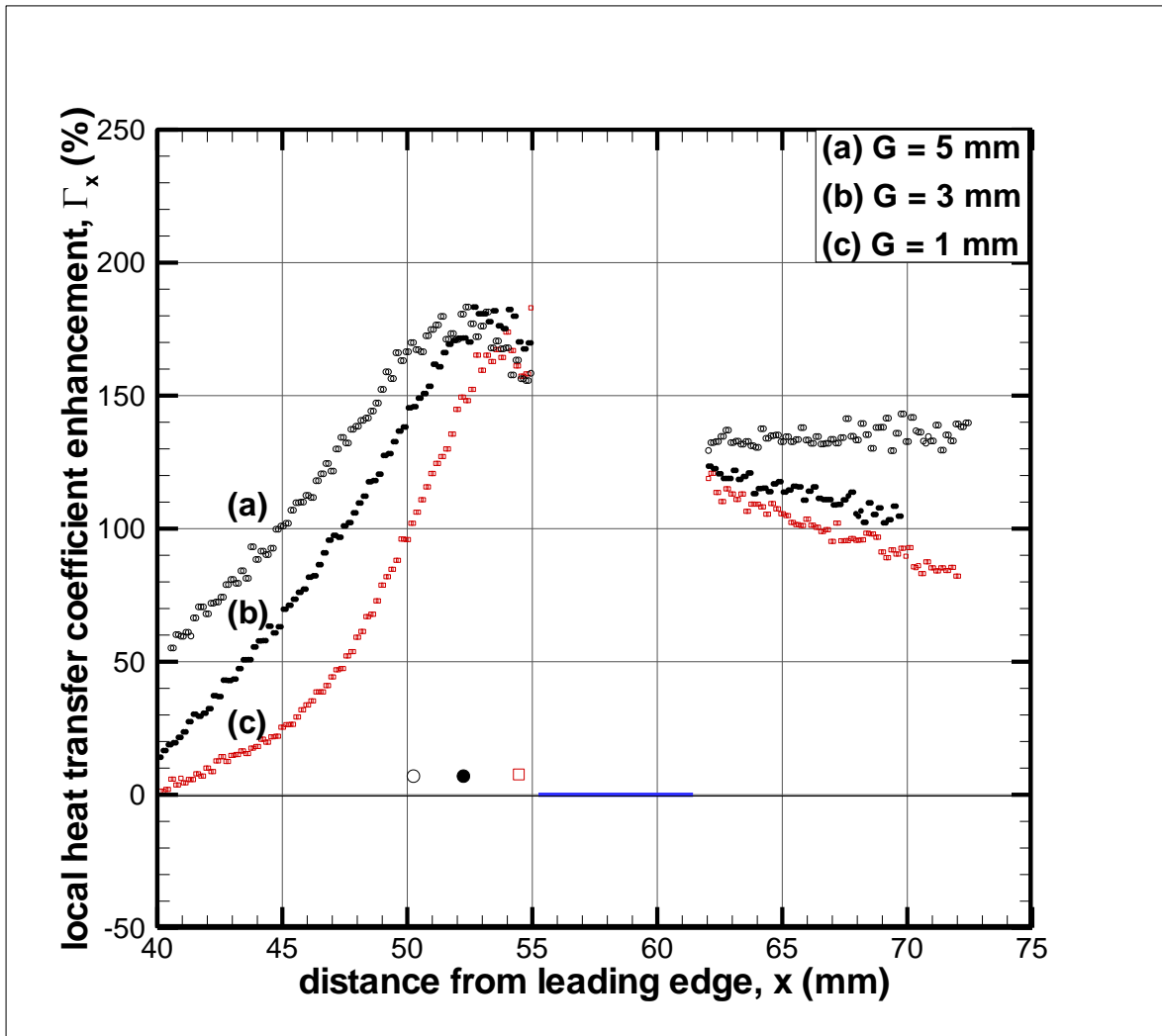


Figure 8 Percentage increase in local heat transfer coefficient for three electrode gaps at a constant electrode height of $H = 3.15$ mm. The bulk velocity was $u = 0.28$ m/s, and the heater power was $P = 4$ W. The blue line represents the collecting electrode, and the three dots represent the different positions of the corona wire for different electrode gaps.